

# Investigation into SNR-accelerated CRs at the prospect of future MeV $\gamma$ -ray detectors

Bing Liu<sup>1,2,3</sup>, Rui-zhi Yang<sup>1,2,3</sup>, Jia-hao Liu<sup>1,2,3</sup>, Xin-yu He<sup>3,4</sup>, Felix Aharonian<sup>5,6,7</sup>

SNRs are thought to be the most prominent CR accelerators in our Galaxy. The renaissance of MeV  $\gamma$ -ray astronomy (e-ASTROGAM, AMEGO, COSI, MeGaT, MeVGRO, MASS, MeVCube, GRAMS, GECCO, HARPO, SMILE-3...) may allow us:

- study SNR accelerated low-energy CRs (LECRs,  $<1$  GeV/nucleon) via MeV nuclear de-excitation line emission resulting from inelastic collisions between LECR nuclei and the medium gases (such as the 4.44 MeV line from  $^{12}\text{C}$  and the 6.13 MeV line from  $^{16}\text{O}$ ), derive unique information about the injection of LECR nuclei from SNRs with the advantage of excluding the influence of CR electrons.
  - perform more precise measurements of pion-bump structure and provide unique information on the acceleration and confinement of high-energy particles. Although pion-bump was found in SNR W44 and IC443 by AGILE and Fermi-LAT, but the results was controversial due to uncertainties of the spectral data, more precise measurements of the  $\gamma$ -ray spectra around 10-100 MeV can help us distinguish the bremsstrahlung emission from pion-decay mission ...
- Given the performance of next-generation MeV  $\gamma$ -ray detectors, we take SNR Cas A and W44 as representatives to discuss the possible detection of nuclear de-excitation lines from SNR-accelerated CRs and precise measurement of pion-bump structure.

## Possible nuclear de-excitation line emission from SNR Cas A

### Assumption for the MeV line calculation

#### CR proton Spectra

Studies of nonlinear shock acceleration predict that the spectra of the accelerated particles show some concavity in momentum space.

$$F(E) = \begin{cases} N_0 \left[ \frac{p(E)}{p(E_b)} \right]^{-\alpha_1} \exp \left[ -\frac{p(E)}{p(E_{\text{cut}})} \right], & \text{if } E \geq E_b \\ N_0 \left[ \frac{p(E)}{p(E_b)} \right]^{-\alpha_2} \exp \left[ -\frac{p(E)}{p(E_{\text{cut}})} \right], & \text{if } E < E_b \end{cases}$$

$$E_{\text{cut}} = 10 \text{ TeV}, E_b = 0.2 \text{ GeV}, \alpha_1 = 2.0 - 2.7, \alpha_2 = \alpha_1 + 3.0, 4.0$$

#### Compositions of interacting medium

Case 1: ejecta only

Case 2: circumstellar medium (CSM)

Case 3: 50% ejecta + 50% CSM

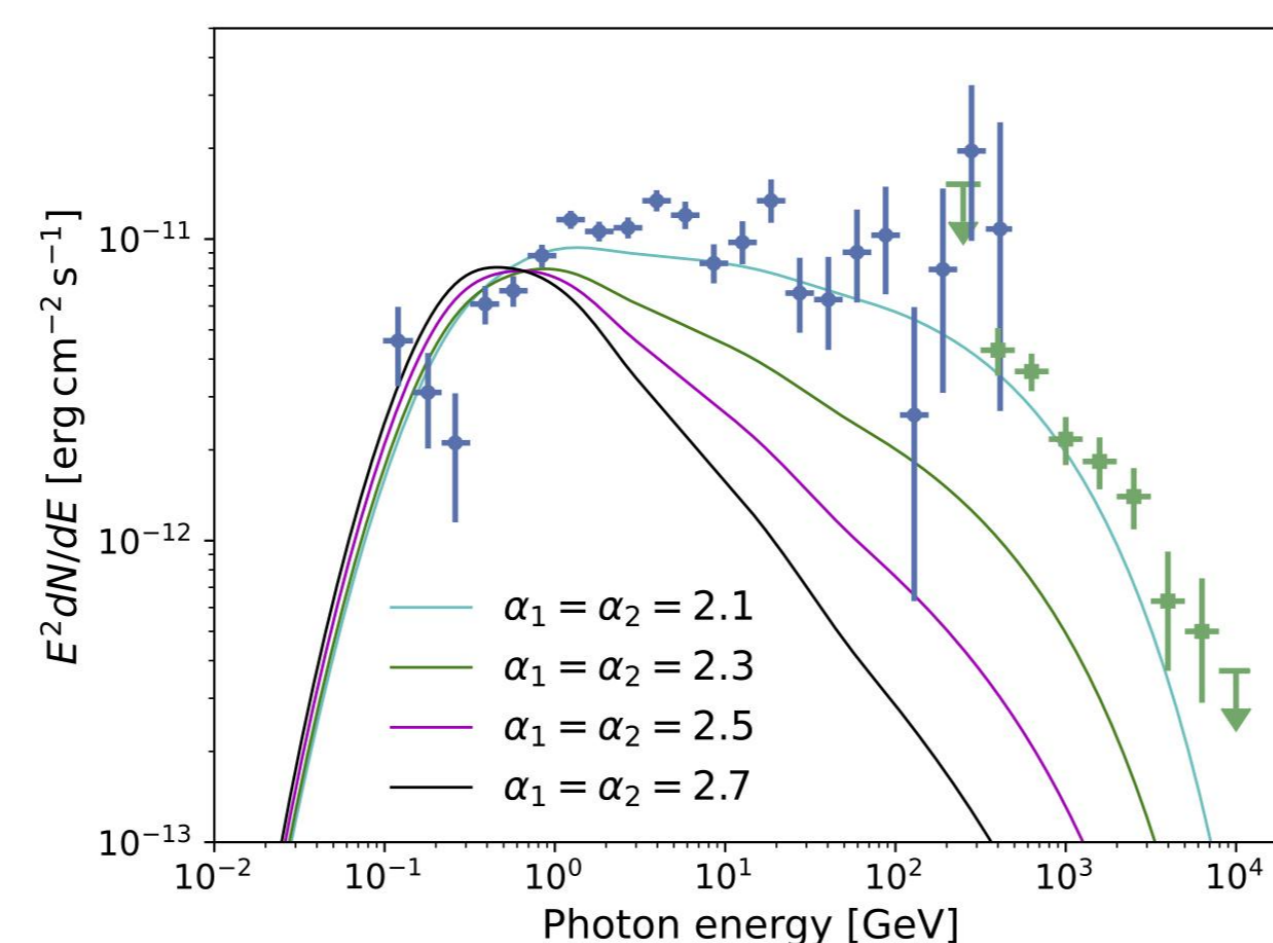


Fig.1 Examples of the hadronic  $\gamma$ -ray emission from Cas A with various assumptions of  $\alpha_1$  and  $\alpha_2$ . The CR proton flux is constrained by GeV-TeV observation data from Abeyssekara et al. 2020.

## Precise measurement of pion-bump structure and e/p ratio in the case of SNR W44

### MeV continuum $\gamma$ -rays from SNR W44 for different origin scenarios

The observed  $\gamma$ -ray spectrum from SNE W44 can be explained by both pion-decay (hadronic) emission and bremsstrahlung (leptonic) emission, in the MeV band, the flux can be different by orders of magnitude due to sharp spectral cutoff in the pion-decay  $\gamma$ -ray spectrum.

Even if the GeV  $\gamma$ -rays are mainly hadronic, there will be inevitable bremsstrahlung emission produced by primary electron as well as secondary electrons, which can be even more significant below 100 MeV.

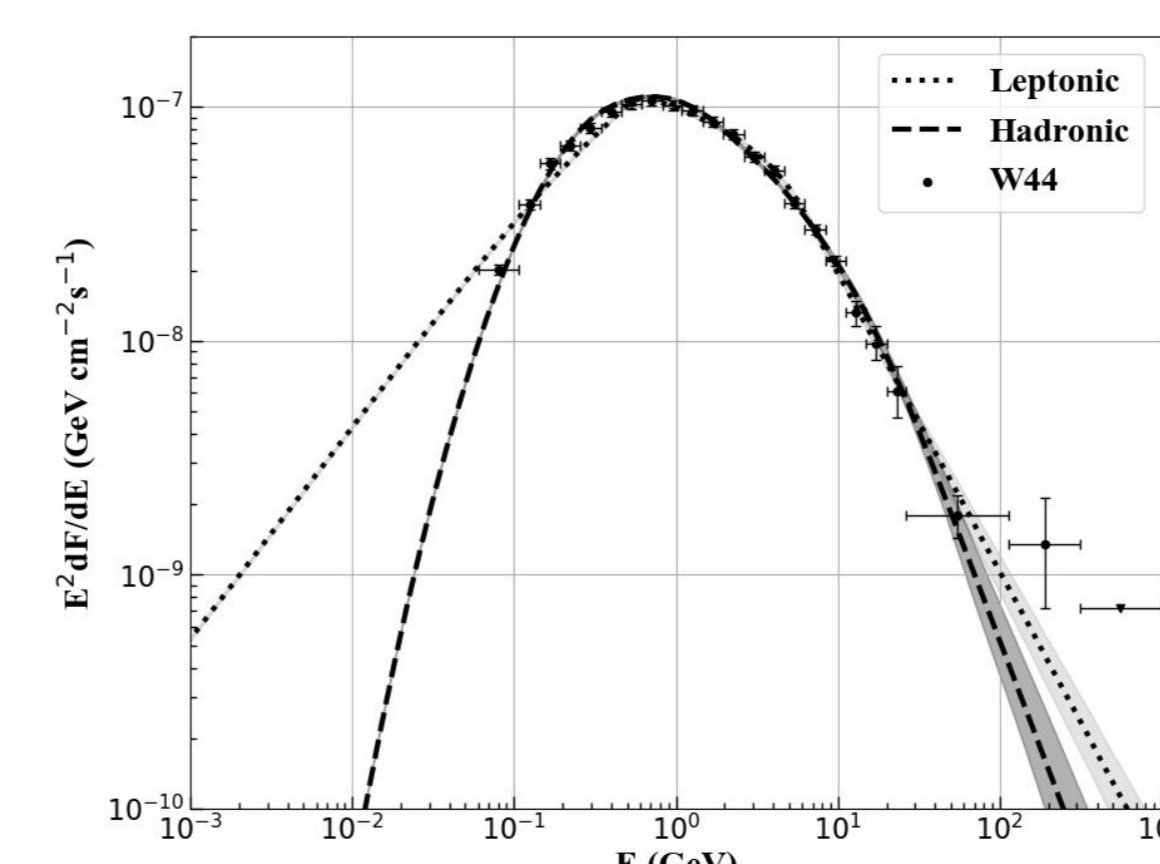


Fig.5 SED of  $\gamma$ -rays from W44. The data points show the observed SED derived from Fermi Pass8 data (Peron et al. 2020).

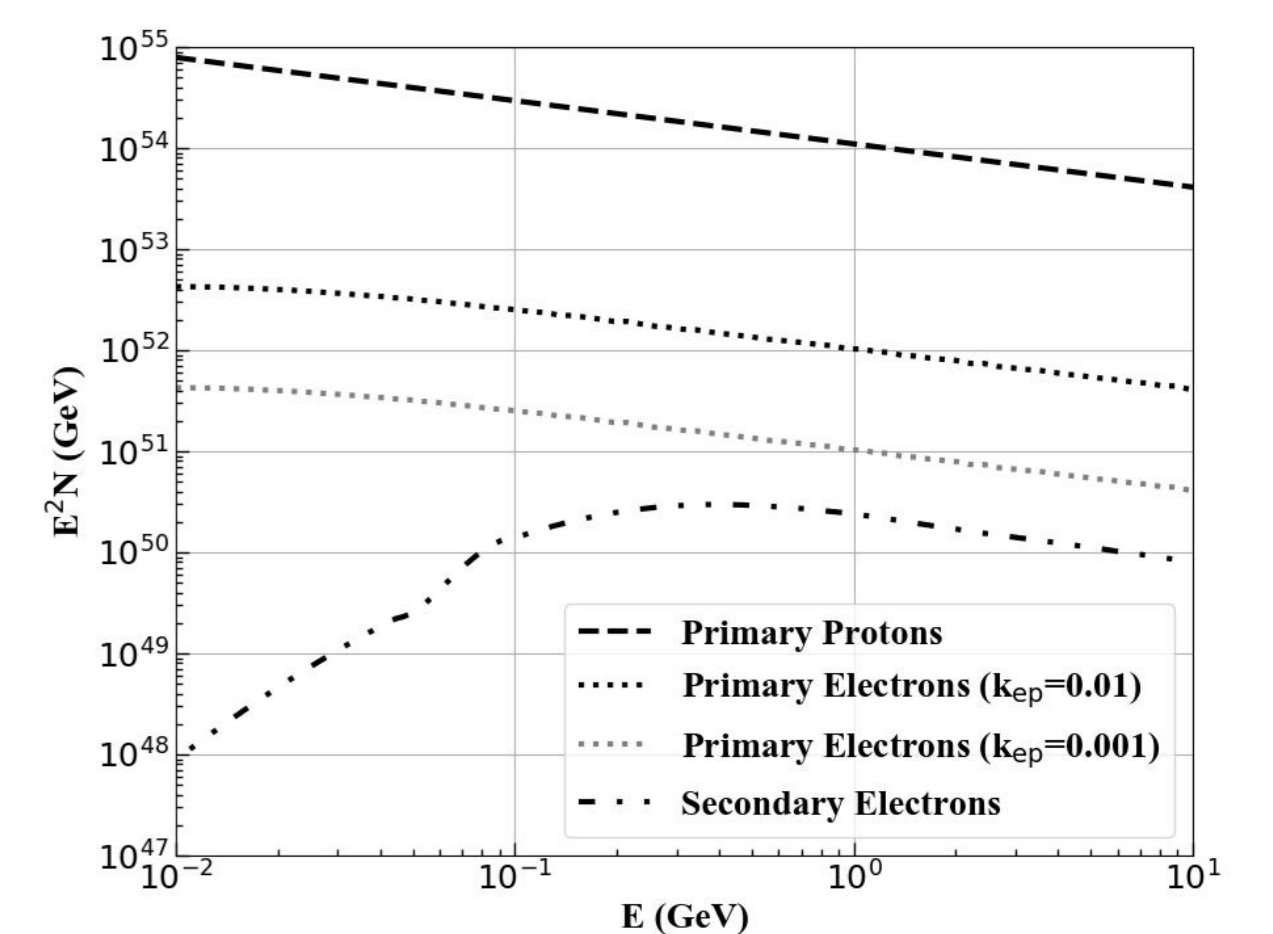


Fig. 6: Estimated energy distributions of the number of different particles after time evolution in the hadronic scenario. The gas density  $n=10 \text{ cm}^{-3}$  and the age of W44  $T=10^{12} \text{ s}$ .

### Calculated MeV nuclear de-excitation line emission for different assumptions

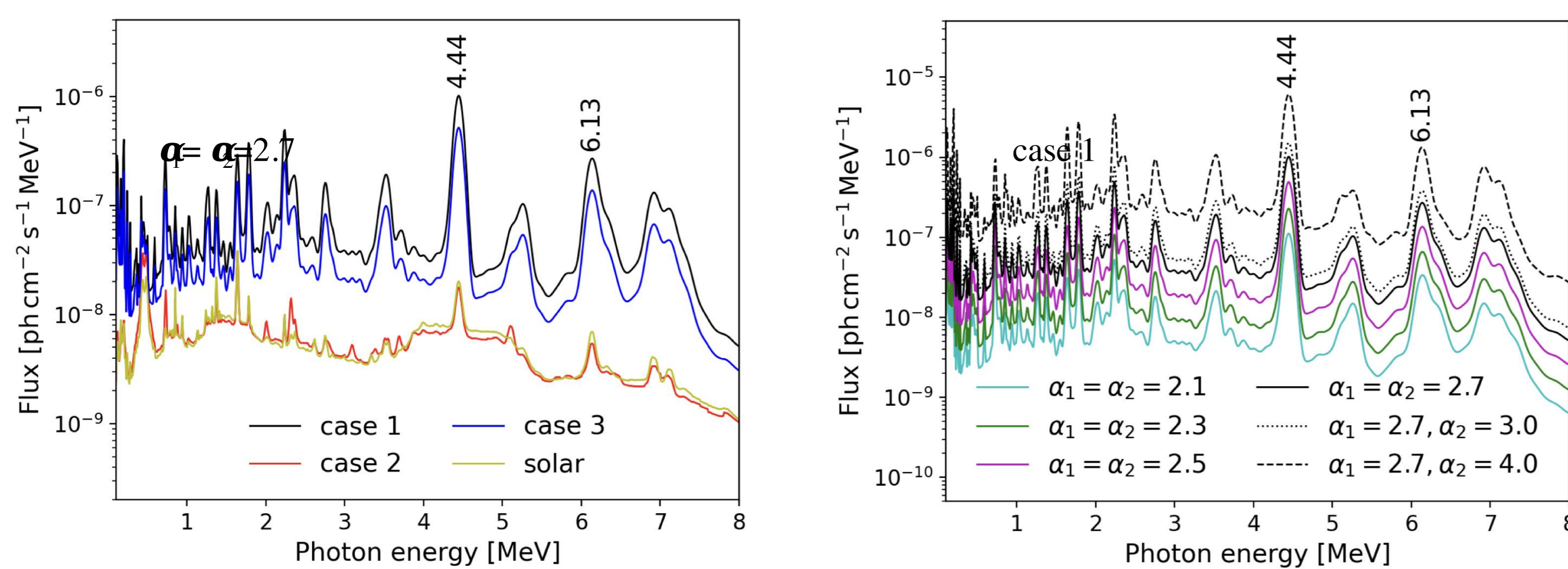


Fig 2. Comparison of estimated MeV  $\gamma$ -ray line emission with different and different interacting medium (case 1: ejecta, case 2: CSM, case 3: ejecta+CSM) and spectral settings of  $\alpha_1$  and  $\alpha_2$ .

### Integrated line fluxes of various cases (without considering the continuum background)

Medium	4.44 MeV	6.13 MeV
case 1 Ejecta	$(0.09-7.71) \times 10^{-7}$	$(0.04-2.10) \times 10^{-7}$
case 2 CSM	$(0.10-8.84) \times 10^{-9}$	$(0.04-2.66) \times 10^{-9}$
case 3 Ejecta + CSM	$(0.05-3.93) \times 10^{-7}$	$(0.02-1.06) \times 10^{-7}$

### Detectability against the MeV continuum background

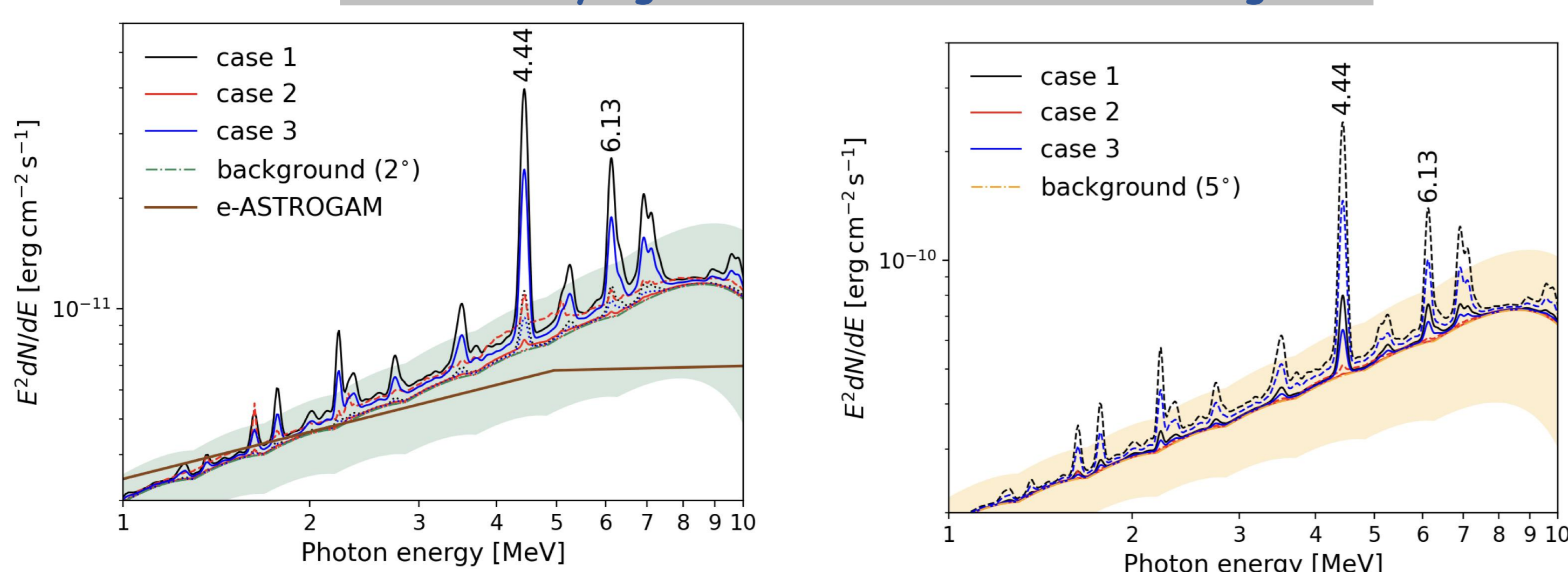


Fig.3 The overall MeV  $\gamma$ -ray emission from Cas A region with extrapolated diffuse background (Siegert et al. 2022) added for various cases and spectral shapes ( $\alpha_1 = \alpha_2 = 2.7$ : solid lines,  $\alpha_1 = \alpha_2 = 2.1$ : dotted line,  $\alpha_1 = 2.7, \alpha_2 = 4.0$ : dashed lines). The shaded area represents possible diffuse background emission around Cas A, assuming the angular resolutions of the telescope are  $2^\circ$  (green) or  $5^\circ$  (orange).

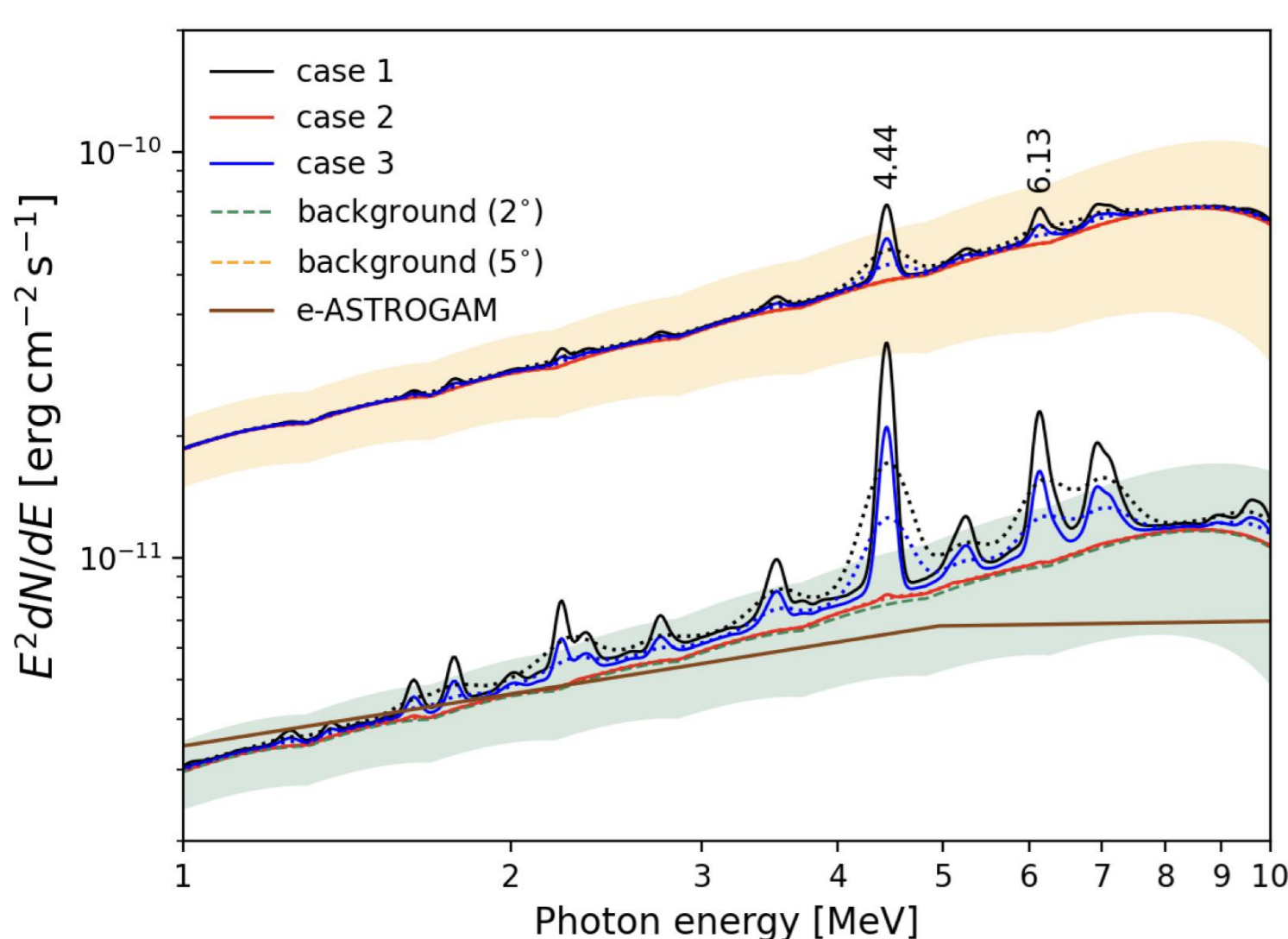


Fig.4 The overall MeV  $\gamma$ -ray emission from Cas A region with extrapolated diffuse background added assuming the energy resolutions of the detectors ( $\Delta E/E$ ) are 2% (solid lines) and 10% (dotted lines), respectively. The sensitivity of e-ASTROGAM calculated at 3 for an effective exposure of 1 year and for a source at high Galactic latitude is shown by the brown line (de Angelis et al. 2018).

### Summary

The predictions of the flux and spectral shape of the MeV line emission from SNR Cas A is highly model-dependent. Good sensitivities and angular resolutions are required to detect the nuclear line emission with flux  $\sim 10^{-7}-10^{-6} \text{ ph/cm}^2/\text{s}$  and for the continuum with energy flux  $\sim 10^{-11} \text{ erg/cm}^2/\text{s}$ .

### Detectability of next-generation MeV instruments

#### Estimation of future observation data (1-100 MeV, 4 energy bins, Poisson distribution)

Assumed performance of the instruments:

Effective area  $A_{\text{eff}}$ : 100  $\text{cm}^2$ ,

Angular resolution:  $1^\circ$  at 10 MeV

Observation time  $T_{\text{obs}}$ : 2 months

$$N_{\text{counts}} = \int_{E_{\text{lower}}}^{E_{\text{upper}}} F(E) T_{\text{obs}} A_{\text{eff}}(E) dE$$

$$\sigma = \sqrt{N_{\text{total}}} = \sqrt{N_{\text{signal}} + N_{\text{bkg}}} \quad S = \frac{N_{\text{signal}}}{\sqrt{N_{\text{signal}} + N_{\text{bkg}}}}$$

$$F_{\text{up}} = \frac{N_{\text{signal}} + 3\sqrt{N_{\text{signal}} + N_{\text{bkg}}}}{A_{\text{eff}}(E_{\text{mid}}) T_{\text{obs}} (E_{\text{upper}} - E_{\text{lower}})}$$

$N_{\text{counts}}$ : the data counts of each bin

$E_{\text{lower}}/E_{\text{upper}}$ : lower/upper bond of the energy bin

$F(E)$ : the theoretical differential flux

$N_{\text{bkg}}$ : The diffuse background was estimated by

combing the extrapolating data form INTEGRAL

observation (Siegert et al.2022) and Fermi-LAT

analysis data using interstellar emission model

gll\_iem\_v07.fits

$\sigma$  the uncertainty of the data

S: the significance of the data,  $\propto \sqrt{T_{\text{obs}}}$

$F_{\text{up}}$ : the 3 $\sigma$  upper limit

Predicted  $\gamma$ -ray counts of future observation for the leptonic scenario shown in Fig.5 (left) and the hadronic scenario in which the bremsstrahlung from primary electrons is added and different e/p ratio is considered (right).

log(E/MeV)	$N_{\text{signal}}$	$N_{\text{bkg}}$	S ( $\sigma$ )	$N_{\text{signal}}$			
				e/p=0.01	e/p=0.001	e/p=0.01	e/p=0.001
0.0-0.5	306	3099	5.24	2676	268	35.21	4.62
0.5-1.0	274	1954	5.80	583	60	11.57	1.34
1.0-1.5	245	763	7.72	137	28	4.57	1.00
1.5-2.0	213	236	10.05	116	95	6.19	5.23

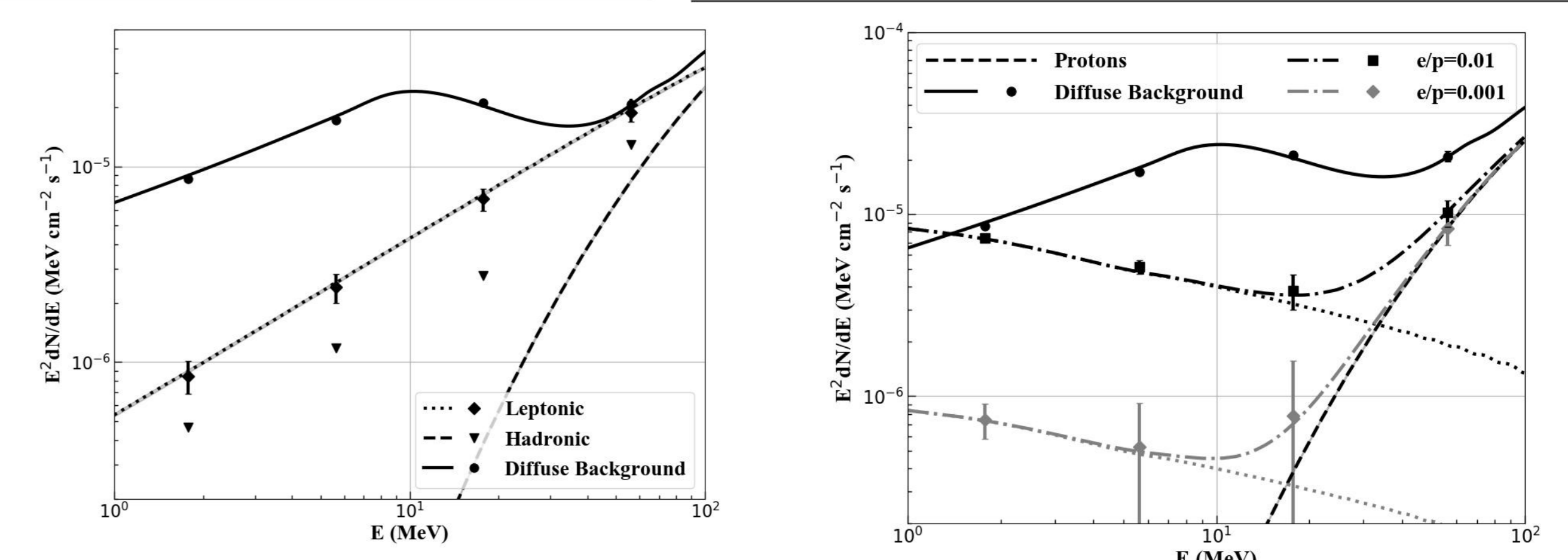


Fig. 7 Estimated SED of future MeV  $\gamma$ -ray observations of W44 for different scenarios. Left panel: comparison of pion-decay  $\gamma$ -rays and bremsstrahlung  $\gamma$ -rays derived from Fermi-LAT data. Right panel: comparison of the hadronic  $\gamma$ -ray spectra (pion-decay  $\gamma$ -rays + bremsstrahlung  $\gamma$ -rays from primary electrons) with different e/p ratio (0.01 or 0.001). The dashed lines show  $\gamma$ -ray fluxes of the pion-decay process, the dotted lines shows the flux from the bremsstrahlung of electrons, and the chain lines show the summed flux from both primary electrons and primary protons. The data points and error bars show the derived flux and 1 $\sigma$  uncertainty of the 4 energy bins. The inverted triangles show the 3 $\sigma$  upper limit of the flux of  $\gamma$ -rays for hadronic scenario shown in Fig.5 (only pion-decay emission from protons).

### Summary

For the specific case of W44, the dedicated MeV investigations using future MeV detectors can significantly improve the ability to distinguish the pion-decay bump from the Bremsstrahlung emissions of CR electrons. In case the pion-decay bump is confirmed, the precise observation of  $\gamma$ -ray spectrum below the pion-decay bump can provide a direct measurement of e/p ratio in the accelerated CR in W44. Even after taking into account the diffuse background, a marginal exposure of 2 months would be enough for such kind of study for planned MeV detectors with  $A_{\text{eff}} \sim 100 \text{ cm}^2$  and angular resolution of  $1^\circ$  at  $\sim 10 \text{ MeV}$ . For other older accelerators with higher ambient density, the MeV observations can also provide clues on the particle confinement near the accelerators.

1 Deep Space Exploration Laboratory/School of Physical Sciences, University of Science and Technology of China, Hefei 230026, China

2 CAS Key Laboratory for Research in Galaxies and Cosmology, Department of Astronomy, School of Physical Sciences, University of Science and Technology of China, Hefei, Anhui 230026, China

3 School of Astronomy and Space Science, University of Science and Technology of China, Hefei, Anhui 230026, China

4 Key Laboratory of Dark Matter and Space Astronomy, Purple Mountain Observatory, Chinese Academy of Sciences, Nanjing 210023, China

5 Dublin Institute for Advanced Studies, 31 Fitzwilliam Place, Dublin 2, Ireland

6 The Max-Planck-Institut für Kernphysik, P.O. Box 103980, D 69029 Heidelberg, Germany

7 Gran Sasso Science Institute, 7 viale Francesco Crispi, 67100 L'Aquila, Italy